

Article

Distribution of Copper, Iron, and Sulfur in Copper Concentrate Particles during Oxidation under Simulated Flash Smelting Conditions

Manuel Pérez-Tello¹, Valeria de la Paz-Ojeda¹, Víctor R. Parra-Sánchez^{2,*} , Eugenia A. Araneda-Hernández², Madrioly C. Fernández-Sagredo² and Eduardo A. Villagrán-Guerra²

¹ Department of Chemical Engineering and Metallurgy, University of Sonora, Boulevard Luis Encinas & Rosales Col. Centro, Hermosillo 83000, Mexico; manuel.perez@unison.mx (M.P.-T.); valeriadelapazo@hotmail.com (V.d.l.P.-O.)

² Department of Metallurgical Engineering, University of Concepcion, Edmundo Larenas 285, Barrio Universitario, Concepción 4030000, Chile; euaraned@udec.cl (E.A.A.-H.); madfernandez@udec.cl (M.C.F.-S.); eduvillagran@udec.cl (E.A.V.-G.)

* Correspondence: vparras@udec.cl; Tel.: +56-989621095

Abstract: The distribution of copper, iron, and sulfur during the oxidation of La Caridad copper concentrate particles under simulated flash smelting conditions was studied in a laboratory reactor. Six wet-sieved size fractions and the unsieved copper concentrate were oxidized at 1123 K and 40% and 70% O₂ by volume in the process gas during the experiments. Samples of partially oxidized particles were collected at 0.2, 0.8, and 0.9 m from the point of entry and analyzed in a QEMSCAN[®] unit to determine the elemental composition within the population of particles. The distribution of the major elements during oxidation was strongly dependent upon the size and chemical composition of the initial particles. Overall, the copper content tended to increase and sulfur content decreased along the reactor length within all sizes. In contrast, the distribution of iron did not follow a general trend, as it was found to increase, decrease, or remain unchanged depending on the particle size. This finding may represent a key feature to further investigate the reaction path followed by particles during flash smelting, especially those associated with particle fragmentation. In general, the larger the particle size was, the larger the change in the content of the major elements within the particle population. Based on the experimental results, particles within a size fraction of <45 μm tended to follow a reaction path consisting of rapid melting followed by the collision and coalescence of reacting droplets during flight. In contrast, particles within the fraction of 45–53 μm tended to react individually. The oxidation behavior of the unsieved concentrate particles showed a combination of both reaction paths.

Keywords: flash smelting; copper concentrate; distribution of elements; oxidation; particle size evolution; dust; collision and coalescence



Citation: Pérez-Tello, M.; de la Paz-Ojeda, V.; Parra-Sánchez, V.R.; Araneda-Hernández, E.A.; Fernández-Sagredo, M.C.; Villagrán-Guerra, E.A. Distribution of Copper, Iron, and Sulfur in Copper Concentrate Particles during Oxidation under Simulated Flash Smelting Conditions. *Minerals* **2024**, *14*, 315. <https://doi.org/10.3390/min14030315>

Academic Editors: Álvaro Aracena Caipa and Hyunjung Kim

Received: 23 January 2024

Revised: 27 February 2024

Accepted: 13 March 2024

Published: 16 March 2024



Copyright: © 2024 by the authors. Licensee MDPI, Basel, Switzerland. This article is an open access article distributed under the terms and conditions of the Creative Commons Attribution (CC BY) license (<https://creativecommons.org/licenses/by/4.0/>).

1. Introduction

The flash smelting process (FSP) is the predominant technology by which metallic copper is currently produced from sulfidic raw materials in the world. In the process, finely divided copper concentrate particles (5–200 μm) enter the reaction shaft of the flash smelting reactor, where they are oxidized with an oxygen-enriched gas stream at a high temperature (1473–1673 K). Upon entering the reaction shaft, the particles are heated up by radiation from the furnace walls and by interface heat transfer from the surrounding gas. The particles are oxidized as they travel through the reaction shaft. Because the oxidation reactions are highly exothermic, the particles melt before they reach the molten bath. Here, additional interface reactions produce the matte, containing a 70 pct. weight of copper on average, and the slag, which contains most of the iron of the concentrate. The

oxidation of the particles generates SO_2 gas, which is used to produce sulfuric acid as a by-product. Despite the fact that the FSP is considered a consolidated technology, a number of phenomena occurring within the flash smelting furnace are yet not understood [1]. Of particular relevance are the uncertainties in the physical and chemical changes experienced by the particles during flight in the reaction shaft. Such a sequence of transformations along the particle trajectory is usually referred to in the literature as the reaction path. This may include size changes such as fragmentation, agglomeration, collision and coalescence of droplets, and chemical transformations, as well as the exchange of momentum, heat, and mass transfer under highly turbulent conditions. The elucidation of the reaction path in the reaction chamber of the flash smelting furnace is relevant because it has strong implications for the reactor's performance. It is also related to common operation problems faced by process engineers, such as the generation of large amounts of dust, the thermal control of the reactor, recovery of valuable metals, and emissions reduction, among other issues.

The reaction path of sulfide particles in a flash smelting reactor has been studied by several authors in the literature [2–10]. The experimental approach typically involves the use of a laminar flow reactor in which oxidation tests are conducted under controlled laboratory conditions. A few studies [11–13] have also been conducted in pilot-plant facilities. A thorough review on the subject was included in a recent publication by Perez-Tello et al. [14]. Thus, only a brief summary is provided here. Overall, the reaction path is strongly dependent upon the chemical composition of the particles and the density of the particle–gas suspension. At a low density of the particle–gas suspension, the particles may be assumed to react individually and, thus, no particle–particle interactions occur. In such a case, the reaction path originally proposed by Kim and Themelis [2] and further modified by Jokilaakso et al. [9] is widely accepted to explain most of the experimental observations. The model is shown in Figure 1 and assumes that the oxidation starts at the particle surface, forming a porous crust of oxide products surrounding the unreacted core of sulfides. The heat of the exothermic reactions causes the particle temperature to increase rapidly until the sulfide core melts. The sulfur dioxide gas produced by the oxidation reactions accumulates as bubbles within the molten core. As the bubbles coalesce and grow, the pressure inside the particle increases. When the internal pressure overcomes the resistance of the oxide crust, the particle undergoes fragmentation. The extent to which fragmentation occurs strongly depends on the oxidation conditions prevailing in the reactor. In an alternative path, the particle melts completely before significant oxidation occurs. The droplets thus formed disintegrate violently.

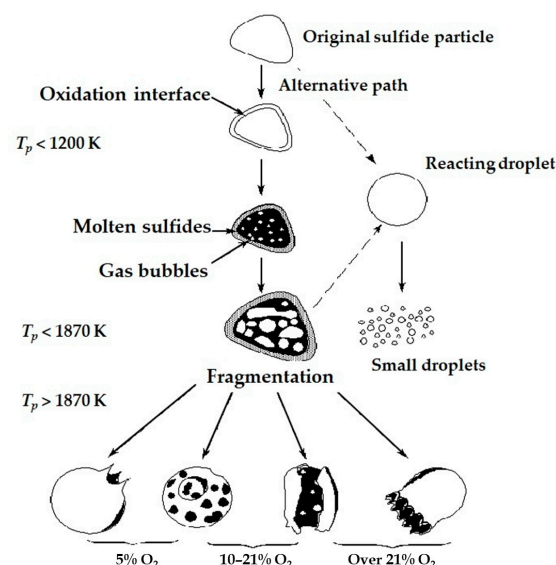


Figure 1. Reaction path of sulfide particles during flash smelting assuming low density of the particle–gas suspension. Adapted from references [9,15].

On the other hand, under conditions of high density of the particle–gas suspension, the probability of particle–particle collisions increases, and a possible mechanism is shown in Figure 2. This was adapted from the original model proposed by Themelis et al. [16] and is supported by recent microscopic observations made in this laboratory [14]. Here, the particles become fully molten shortly after they enter the reaction chamber. Because the number of droplets being formed is very high, they collide with each other and form larger droplets by coalescence. Under such conditions, the collision and coalescence of the droplets occur simultaneously with the oxidation reactions. Because the coalescence of droplets gradually decreases the surface area available for gas–liquid contact in the particle population, this reaction path is deleterious for the elimination of sulfur from the reacting droplets. Figures 1 and 2 may represent the two extremes of reaction paths in an industrial flash smelting furnace. Because the density of the particle–gas suspension is not uniform throughout the reaction shaft, it is likely that both mechanisms occur simultaneously at different locations in the reactor.

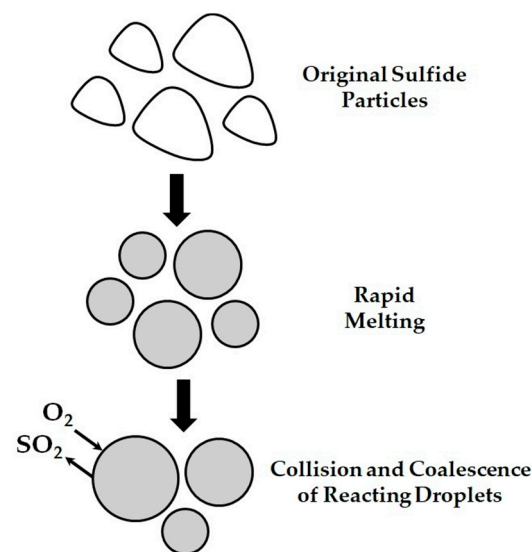


Figure 2. Reaction path of sulfide particles during flash smelting assuming high density of the particle–gas suspension. Adapted from references [14,16].

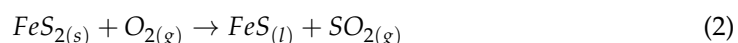
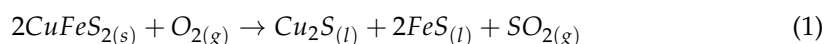
The present work continues the previous study on the oxidation of copper concentrate particles conducted in this laboratory [14]. Some relevant findings of that study included the following: (1) the chemical composition of the initial particles was strongly size-dependent; (2) the smallest size fraction in the feed ($<45\ \mu\text{m}$) tended to create particles that were larger than the original sizes, whereas particles with sizes of $>45\ \mu\text{m}$ tended to fragment and produce dust particles ($<20\ \mu\text{m}$); (3) the smallest particles in the feed ($<45\ \mu\text{m}$) showed lower reactivity than larger particles ($>45\ \mu\text{m}$); and (4) the oxidation behavior of unsieved concentrate particles showed trends of both small ($<45\ \mu\text{m}$) and large ($>45\ \mu\text{m}$) particles in the feed. The overall observations were explained in terms of a series of chemical reactions and the mechanisms shown in Figures 1 and 2.

It is noted that the above trends represent the behavior of the particle population as a whole. Furthermore, it was of interest to investigate the evolution of the chemical composition of the reacting particles within the particle population along the laboratory reactor. The first step to achieve this goal is by measuring the content of the major elements in the particles by means of a sophisticated electron microscopic analysis technique in a reduced number of particles from the population collected along the reactor. Furthermore, the goal of this investigation was twofold: first, to analyze the distribution of copper, iron, and sulfur within the particle population of copper concentrate particles oxidized under simulated flash smelting conditions, and second, to correlate the trends observed in the distribution of the major elements with the reaction path followed by the particles in the reactor.

2. Materials and Methods

2.1. Experimental Work

Details of the experimental setup used in the oxidation tests are described elsewhere [14]. Thus, a brief description is provided here. The experimental system consisted of a solid feed unit (SFU), a gas feed unit, a reaction shaft, a product receptacle, and a gas-cleaning unit. The SFU consisted of a vibrating feeder and a water-cooled solid feed lance aligned with the centerline of the reaction chamber. The lance was mobile so that it could penetrate the reactor to a prespecified position. This allowed for control of the residence time of the particles in the reaction chamber. The process gas was provided by two cylindrical vessels containing pure oxygen and nitrogen, which were connected to two rotameters to set the flow rate. The reaction shaft consisted of a vertical ceramic tube heated by two electrical resistances embedded within the tube. The reacting particles were collected using a stationary water-cooled receptacle placed at the outlet of the reaction chamber. The experimental conditions were established based on the following overall chemical reactions:



which represent the main goal of the flash smelting process, i.e., the production of copper matte. During the experiments, the amount of oxygen supplied to the furnace was 1.3 times the stoichiometric amount calculated for reactions (1) and (2), and the oxygen concentration was set to volumes of 40 and 70%. Copper concentrate from La Caridad, Mexico, was used as raw material. Six wet-sieved size fractions and the unsieved concentrate were used for the oxidation tests. In a typical experiment, the reactor was first heated up to 1123 K, and the SFU was set to the prespecified position for the run. Next, the oxygen and nitrogen flow rates were set, and the oxidizing gas mixture was injected into the reactor. During the experiments, both particles and gas traveled downwards through the reaction chamber. The chemical composition of the particles was determined by atomic absorption spectroscopy techniques (Cu and Fe) and gravimetric methods (S and SiO₂). Selected samples were also analyzed by a quantitative evaluation of minerals by scanning electron microscopy (QEMSCAN[®]) using a Tescan-Vega system (Brno, Czech Republic) model LSH with four energy-dispersive X-ray spectroscopy (EDS) detectors.

The experimental conditions relevant to the present investigation are shown in Table 1. The oxygen concentration values were based on typical operating conditions in the industrial flash smelting reactor. The selection of the size fractions was based on the fact that about 70% of the particle population of the original concentrate was found to be in sizes of less than 53 μm [14]. For comparison purposes, unsieved concentrate particles were also analyzed. The sampling locations included the initial particles (0 m) and three positions along the laboratory reactor at 0.2, 0.8, and 0.9 m from the lance tip.

Table 1. Experimental conditions considered for the present work.

Variable	Value
Oxygen concentration in the process gas, vol pct.	40
	70
Size fraction in the feed, μm	<45
	45–53
	Unsieved
Sampling location from the lance tip, m	0.0
	0.2
	0.8
	0.9

All chemical analyses and size distributions reported in this paper were obtained utilizing a QEMSCAN[®] unit at the University of Concepcion, Chile. For that purpose, a probe of epoxy resin was constructed using about 0.68 g of the sample. Next, the probe surface (7 cm²) was thoroughly polished, and the probe was placed into the QEMSCAN[®] unit. The probe surface was scanned, and the particles were identified, counted, and sorted by size by means of the iDiscover 5.3 data processing software built within the QEMSCAN[®] unit. The scanning resolution was set to 2 μm, representing an area of 2 × 2 μm². Particle size measurements were made in Particle Mineralogical Analysis (PMA) mode by dividing the total sample area into quadrants. The software randomly selected candidate particles to be read, thus separating the particles from the background. Once the particles were selected, a scan was made of each particle, focusing the electron beam and collecting the X-rays emitted by the particle. Each particle was analyzed until the exposed area of each selected particle was completed. In each measurement, both brightness and EDS data were obtained. This information was further processed by the iDiscover 5.3 software (FEI Company, Brisbane, Australia) to obtain the elemental analysis of the selected particle. In a typical analysis, about 30,000 particles, corresponding to each sample location in Table 1, were identified, counted, and analyzed.

2.2. QEMSCAN[®] Data Processing

For each experimental condition in Table 1, the QEMSCAN[®] unit provided the chemical composition and size of particles in the form of a sizeable numerical matrix. Because the number and composition of particles within each size range defined by the QEMSCAN[®] unit varied within a given population, the composition provided by the analysis is the average of all measurements conducted within the given size range. The large quantity of data thus obtained were further processed in Excel to obtain the chemical composition of the major elements (copper, iron, and sulfur) within the particle population. In this work, the experimental data are discussed in terms of the changes in the content of the major elements in the particles. This information was obtained from the following expression:

$$\Delta\omega_{i,j}^z = \omega_{i,j}^z - \omega_{i,j}^0 \quad (3)$$

where $\omega_{i,j}^z$ is the content in the weight fraction of element i in a particle with size j in the population collected at position z in the reactor, and $\omega_{i,j}^0$ is the corresponding composition of element i in a particle with size j in the feed ($z = 0$ m). Consequently, the symbol $\Delta\omega_{i,j}^z$ represents the change in the composition of element i in a particle with size j relative to its value in the feed. In this notation, subscript i represents any of the elements: copper, iron, and sulfur. The selection of Equation (3) to analyze the experimental data was based on the fact that the composition of the feed material was not uniform, even within the sieved fractions, and thus, $\omega_{i,j}^0$ was found to be size-dependent. As will be discussed later in this paper, Equation (3) also allowed the visualization of the major trends in the distribution of the elements during particle oxidation.

3. Results and Discussion

This section is divided into subheadings to provide an organized discussion of the experimental findings.

3.1. Overall Chemical Composition and Size Distribution of the Feed Particles

Figure 3 shows the overall chemical composition of the size fractions and the unsieved concentrate used in this work. As expected for a chalcopyrite-based concentrate, the major elements were copper, iron, sulfur, and silicon. It is noted that the overall chemical composition was not uniform. In general, the copper content decreased as the particle size fraction increased. Also, the amount of iron increased as the particle size fraction increased [14]. The sulfur content followed a similar trend to iron. The chemical composition of the unsieved material was similar to that of the fraction of 45–53 μm.

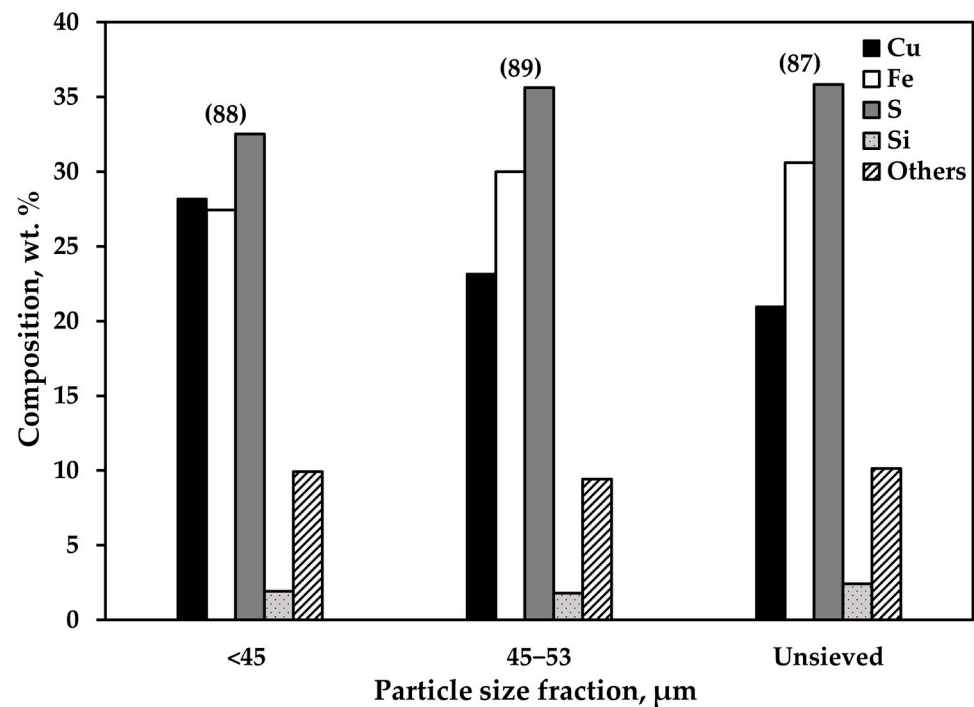


Figure 3. Overall chemical compositions of size fractions of <45 μm and 45–53 μm and the unsieved concentrate. The values in parentheses represent the summation of copper, iron, and sulfur contents.

The major species detected in the particles by X-ray diffraction analysis included chalcopyrite and pyrite, with minor amounts of several copper sulfides and silica. The mineralogical compositions of the size fractions of <45 μm and 45–53 μm and the unsieved concentrate are shown in Table 2 [14]. In general, the smaller the size of the feed was, the higher the content of chalcopyrite was and the lower the pyrite content was. The fact that the chemical composition in the feed was strongly size-dependent is relevant in the present context. This is because the reactivity of mineralogical species is known to be different. Furthermore, this may have implications for the reaction path followed by the particles.

Table 2. Mineralogical compositions of the size fractions of <45 μm and 45–53 μm and the unsieved concentrate, wt.%.

Mineral	<45 μm	45–53 μm	Unsieved
Chalcopyrite, CuFeS ₂	62.0	46.0	46.3
Pyrite, FeS ₂	20.3	35.2	36.4
Chalcocite, Cu ₂ S	6.46	8.01	5.07
Silica, SiO ₂	4.12	4.75	4.61
Others	7.12	6.00	7.67

Figure 4 shows the size distributions measured by the QEMSCAN[®] unit for the size fractions and the unsieved material used in this study. The fraction of <45 μm comprised particles in the range of 3.5 μm to 64.5 μm, i.e., particles larger than the maximum expected size were detected. It is also noted that the volume occupied by the finest particles in the population was small, and most of them were in the range of 3.5 μm to 46 μm. In contrast, the size fraction of 45–53 μm showed the common normal-size distribution shape. The largest size detected in this case was 108 μm. Finally, the volume of particles in the unsieved concentrate was distributed over a wide range of sizes, with a maximum size of 152.5 μm. The mean size of the particle population was calculated using the following equation:

$$\langle x \rangle = \frac{1}{100} \sum_{i=1}^N x_i v_i \quad (4)$$

where N is the number of discretized sizes in the population, and v_i is the percentage in volume of the particle population occupied by size x_i . In this work, any particle within the range of 0 to 20 μm is defined as dust, regardless of its origin and chemical composition. The fraction of <45 μm contained 76% dust, and its mean size was 15.3 μm . In contrast, the volume of dust in the fraction of 45–53 μm was considerably lower (17%) with a mean size of 39.8 μm . Finally, the unsieved concentrate contained 42% dust particles.

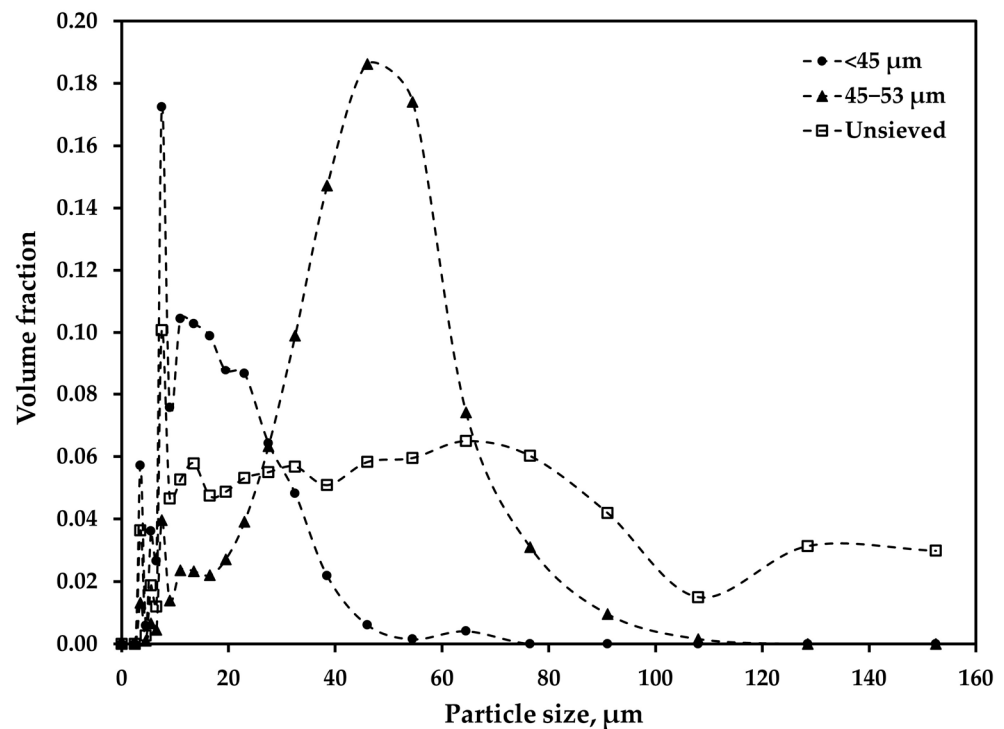


Figure 4. Particle size distributions of size fractions of <45 μm and 45–53 μm and unsieved concentrate determined by the QEMSCAN[®] unit.

Figure 5 shows the distribution of copper as a function of the particle size in the two size fractions and the unsieved concentrate. Most of the experimental values were between the stoichiometric values for chalcopyrite (CuFeS_2) and pyrite (FeS_2), which are shown as references in dashed lines. The copper content in the size fraction of <45 μm showed the lowest variations within the particle population, with a mean value of about 0.30. The fraction of 45–53 μm showed copper content of close to 0.20 in the smallest particles and increased with particle size but keeping values lower than those of the fraction of <45 μm . The values of the copper content in the unsieved material were located at intermediate values relative to the other two fractions. The most significant differences in copper content were observed in dust particles (<20 μm). This suggests that the proportion of the major mineralogical species in such particles may differ from other sizes.

Figure 6 shows the corresponding distributions of iron in the feed material. Here, the experimental data showed lower variability than Figure 5. The experimental values in most of the particles were found to be in the range of the stoichiometric values for chalcopyrite and pyrite. In particles of the order of 100 μm and larger in the unsieved material, the iron content reached values of close to 0.46, corresponding to the stoichiometric content of pyrite. A distinctive feature of Figure 6 is the iron content in dust particles (<20 μm) in all the fractions analyzed, as their values were lower than those of chalcopyrite. A possible explanation is the presence of other copper sulfides, such as chalcocite, in dust particles.

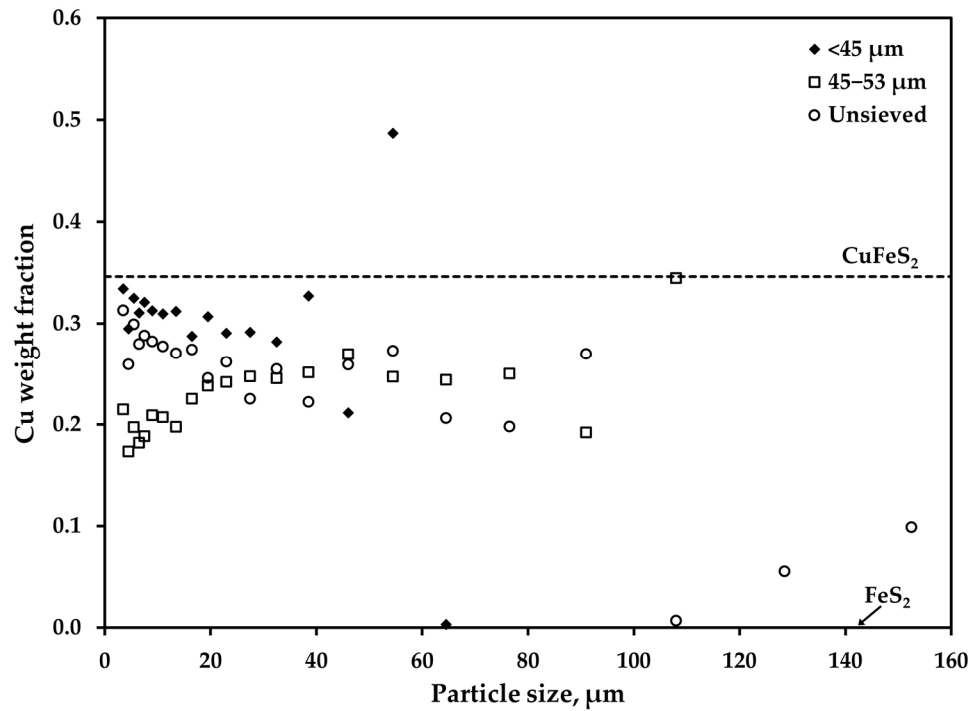


Figure 5. Copper content in the sieved fractions and unsieved La Caridad copper concentrate particles.

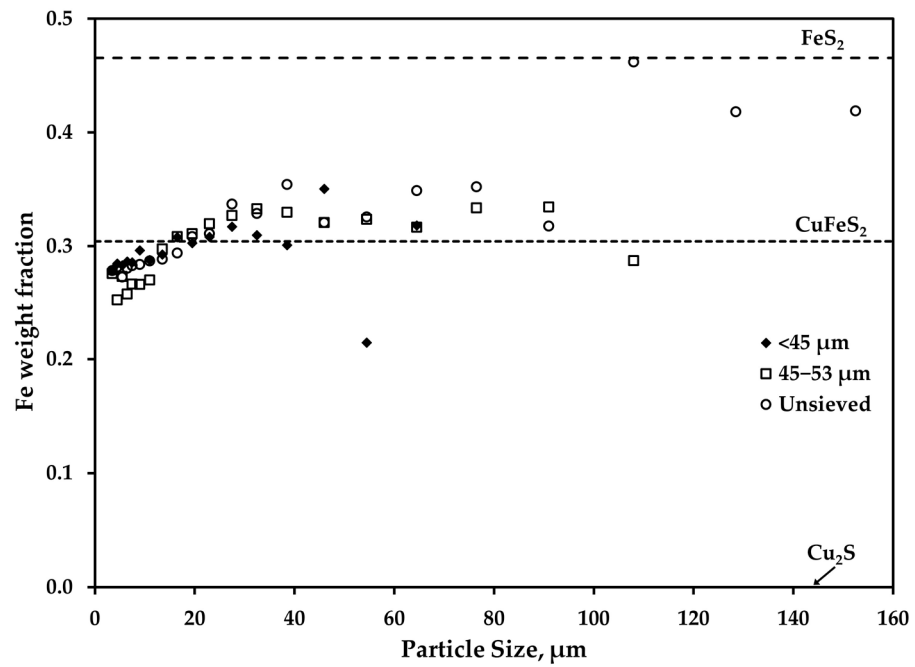


Figure 6. Iron content in the sieved fractions and unsieved La Caridad copper concentrate particles.

Figure 7 shows the distribution of sulfur in the initial particles. Overall, the larger the particle size was, the higher the sulfur content was. The finest particles in the size fraction of 45–53 μm contained less sulfur than other particles. Most of the values in the sieved fractions of <45 μm and 45–53 μm lay within the range of the stoichiometric amounts of chalcopyrite and chalcocite. This is because such fractions contained significant amounts of several copper sulfides and small amounts of iron sulfides. A mineralogical analysis of the samples using the QEMSCAN[®] unit will be the subject of a future publication. Finally, it is noted that the experimental data in Figures 5–7 represent the values of $\omega_{i,j}^0$ on the right-hand side of Equation (3).

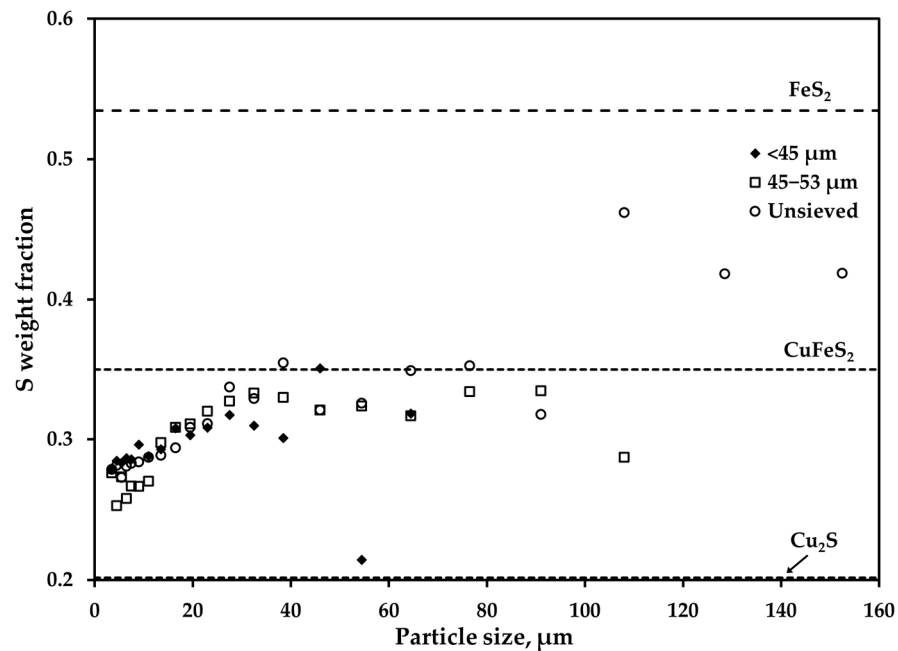


Figure 7. Sulfur content in the sieved fractions and unsieved La Caridad copper concentrate particles.

3.2. Distribution of Major Elements: Size Fraction of $<45 \mu\text{m}$ after Oxidation

Overall, the analysis of the experimental data showed that the oxygen concentration in the process gas did not play a significant role in the distribution of copper, iron, and sulfur when it was varied in the range of 40%–70% in volume [14]. Therefore, the present discussion is only focused on the results obtained under 70% O_2 , as this is the typical oxygen concentration used in industrial operations [17]. Figure 8 shows the change in copper content in the particles within the size fraction of $<45 \mu\text{m}$ that was calculated with Equation (3). For further reference, in this and all the subsequent plots, two dashed lines are added. The horizontal dashed line at zero represents no change in the chemical composition with respect to the feed. Furthermore, any point above or below this reference line indicates that the content of the element at the given particle size either increased or decreased with respect to its value in the feed. The vertical dashed line indicates the largest particle size detected in the feed and was obtained from Figure 4. It is emphasized that the interpretation of Figure 8 cannot be in terms of a Lagrangian approach. This is because particles of any size collected at 0.2, 0.8, and 0.9 m did not necessarily follow the same reaction path, and particles may be created or destroyed according to the reaction paths shown in Figures 1 and 2. The above criteria are also valid in the discussion of the subsequent plots in this paper.

Overall, Figure 8 shows that particles within the size fraction of $<45 \mu\text{m}$, in general, increased their copper content in all sizes with respect to the feed at all sampling locations. Because the copper content increased along the reactor in all sizes, most of the particles in the population likely followed a similar reaction path. Such increase was possibly the result of particle oxidation, which eliminates sulfur and allows oxygen to enter the particle, forming copper and iron oxides. Most of the oxidation reactions proposed in the literature to represent the oxidation of sulfide particles in the flash smelting reactor [10,18,19] involve particle weight loss. Furthermore, the proportions of copper and iron in the particles are expected to increase due to oxidation. It is also noted that the larger the particle size is, the greater the increase in copper content. This behavior is likely due to the differences in the chemical compositions of the feed material, as shown in Figures 5–7. Furthermore, the larger the particles are, the higher the content of pyrite, which is more reactive than chalcopyrite under identical oxidation conditions [19]. A relevant feature in Figure 8 is noted at 0.2 m from the lance tip and farther down the reactor, as new particles of larger than $64.5 \mu\text{m}$ were detected. This suggests that such particles were formed by the collision

and coalescence of partially reacted and molten droplets according to the reaction path shown in Figure 2. This hypothesis was supported by microscopic observation of the reacted particles [14].

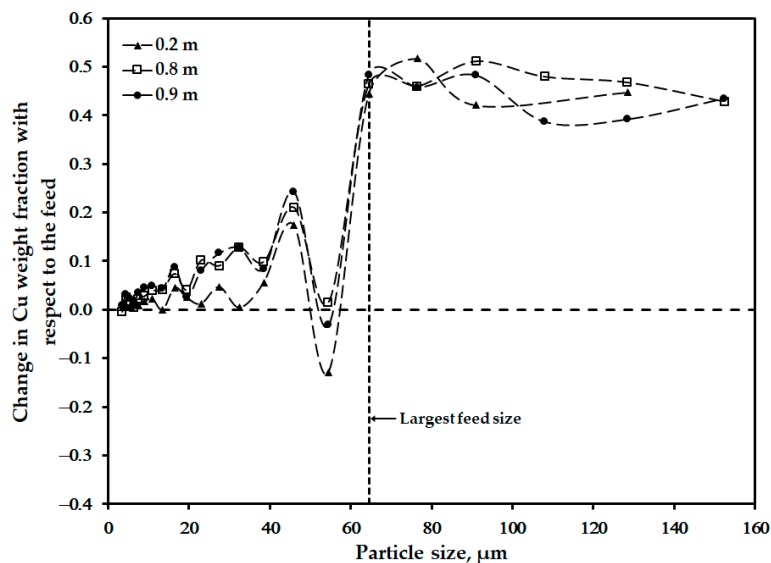


Figure 8. Changes in copper content in particles within the size fraction of <45 μm oxidized under 70 pct. O₂ in the process gas.

Figure 9 shows the corresponding changes in iron content. The behavior of iron deviated from that of copper, as shown in Figure 8. At 0.2 m from the lance tip, the iron content increased substantially with respect to the values in the feed. This occurred in particles with sizes of smaller than about 50 μm. However, at 0.9 m from the lance tip, the iron content in such particles was just slightly higher than their values in the feed. Although this result may seem unexpected, it is recalled that these are Eulerian values. The quantities of free chalcopyrite and free pyrite particles within the size fraction of <45 μm represented 52% and 16%, respectively, of the total population by weight [14]. Therefore, this observation supports the hypothesis that the reaction path followed by the particles was not uniform due to differences in particle composition. Figure 9 also shows evidence of the generation of new particles that were larger than those in the feed containing iron.

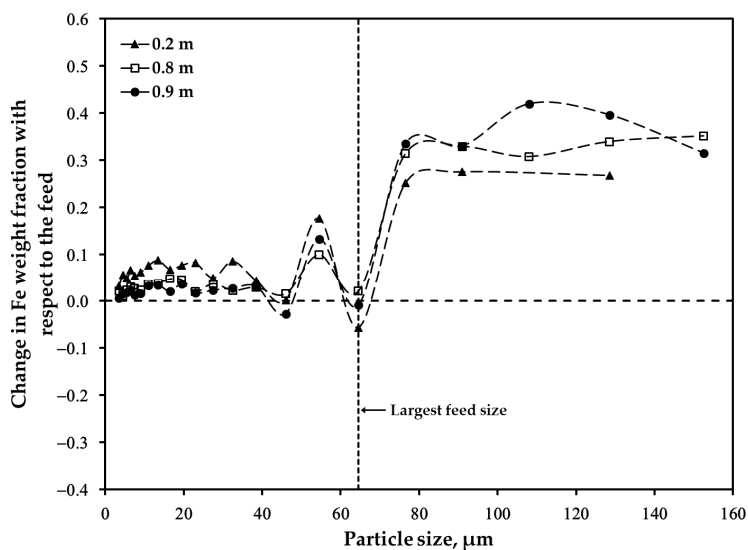


Figure 9. Changes in iron content in particles within the size fraction of <45 μm oxidized under 70 pct. O₂ in the process gas.

Figure 10 shows the changes in sulfur content. Unlike the trends observed in Figures 8 and 9, the sulfur content decreased as the particles traveled through the reaction shaft. This is an expected trend because the flash smelting process aims to eliminate sulfur from the particles. Furthermore, sulfur removal may be considered a quantitative indicator of particle oxidation. The trends observed in Figure 10 are mirror images of those shown in Figure 8. The changes in sulfur content depended on the particle size in the population. All particles began oxidation at 0.2 m. Also, the larger the particle size was, the higher the loss of sulfur. It is noted that the content of sulfur in the new particles formed with sizes of $>64.5 \mu\text{m}$ was similar to that of the initial particles. This suggests that collision and coalescence of droplets occurred between initial and partially reacted particles during flight.

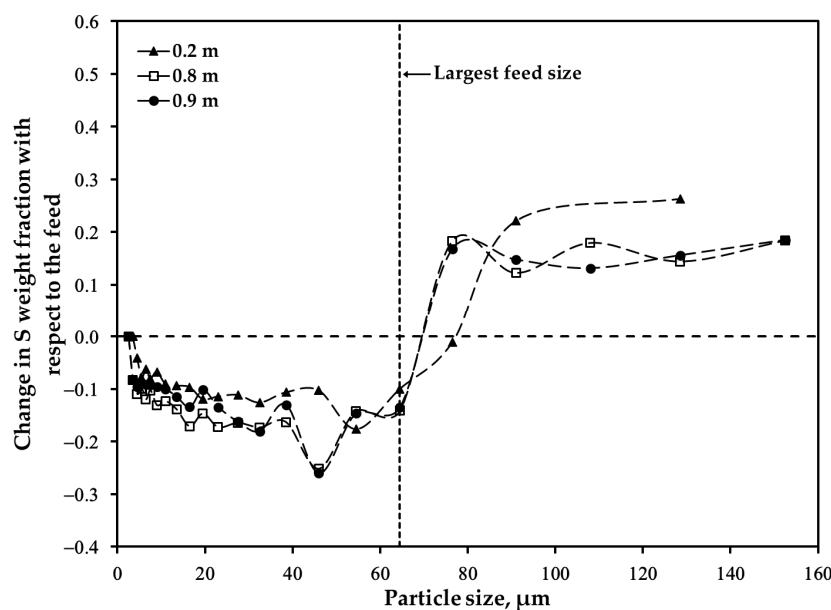


Figure 10. Changes in sulfur content in particles within the size fraction of $<45 \mu\text{m}$ oxidized under 70 pct. O_2 in the process gas.

3.3. Distribution of Major Elements: Size Fraction of 45–53 μm after Oxidation

Figure 11 shows the changes in copper content in particles within the size fraction of 45–53 μm . Significant differences were noted with respect to the trends observed in Figure 8 for the size fraction of $<45 \mu\text{m}$. In this case, the small changes observed at 0.2 m from the lance tip suggest that particle oxidation was initiated farther down the reactor. At 0.8 m, a drastic change in composition was observed, which did not vary significantly at 0.9 m from the lance tip. Again, the larger the particle size was, the greater the copper content increase during oxidation, likely due to the differences in the chemical compositions of the particles in the feed. Unlike the features shown in Figure 8, in this case, no particles larger than the maximum size were detected in the feed. This suggests that particles within this fraction followed the reaction path shown in Figure 1. Figure 11 also shows that the finest particles decreased their copper content with respect to the feed. This was possibly due to the fragmentation of partially oxidized particles, which may produce daughter particles with varying compositions. This hypothesis agreed with previous observations [14], indicating that particles within the size fraction of 45–53 μm produced dust particles upon oxidation.

Figure 12 shows the changes in iron content for particles within the size fraction of 45–53 μm . Significant differences are noted in Figure 9 for the size fraction of $<45 \mu\text{m}$. At 0.2 m from the lance tip, no significant changes in iron content were measured in the particles. This suggests that the oxidation of most particles in the population initiated farther away from the lance tip. At 0.8 and 0.9 m, three ranges of sizes were noted: dust sizes (0 to 20 μm), intermediate sizes (20 to 60 μm), and large sizes (60 to 110 μm). In

general, dust sizes increased their iron content, whereas the intermediate sizes showed no significant changes. Finally, large sizes showed a significant decrease in iron content with respect to their values in the feed. Such behavior points out the complexity of the reaction path followed by the particles and is difficult to explain. A possible explanation is that such changes may be associated with fragmentation phenomena according to the reaction path shown in Figure 1, which may produce daughter particles with varying compositions. However, further investigation is necessary to clarify this point.

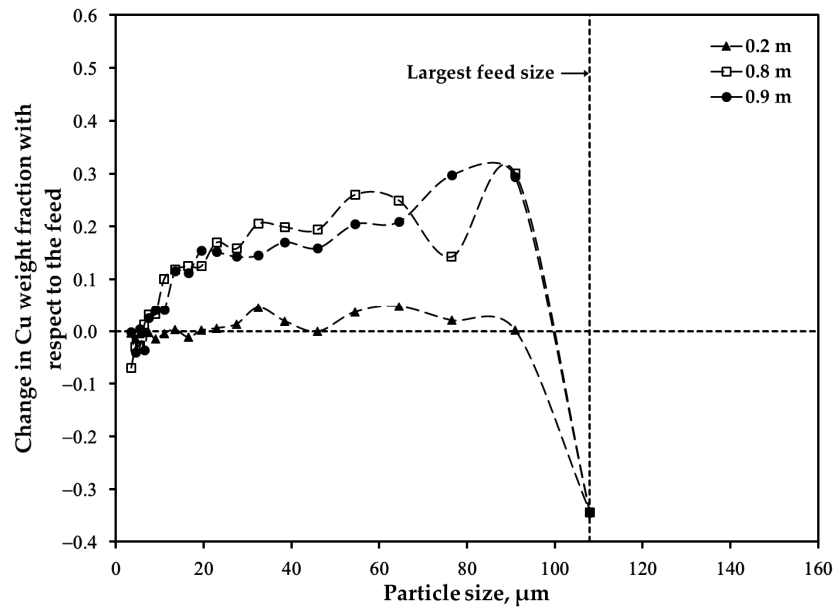


Figure 11. Changes in copper content in particles within the size fraction of 45–53 μm oxidized under 70 pct. O_2 in the process gas.

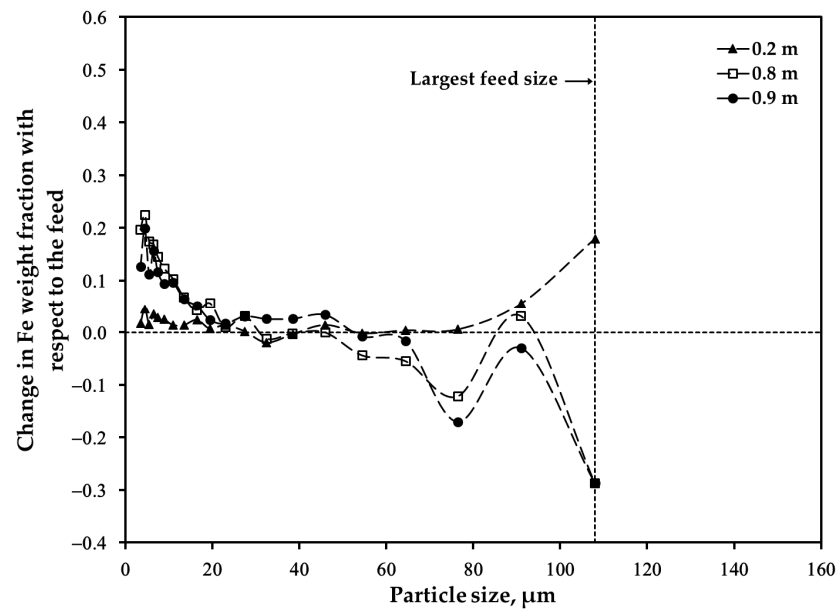


Figure 12. Changes in iron content in particles within the size fraction of 45–53 μm oxidized under 70 pct. O_2 in the process gas.

Figure 13 shows the changes in sulfur content in particles within the size fraction of 45–53 μm . The trends observed agreed well with those shown in Figures 11 and 12. A significant decrease in this quantity was observed at 0.8 m from the lance tip and did not change significantly at 0.9 m. Also, the larger the sizes were, the higher the sulfur depletion

from the particles. Figure 7 showed that dust particles in this size fraction contained less sulfur than other sizes. Figure 13 suggests that dust sizes showed a reaction path essentially different from other sizes, as the loss of sulfur in this range was small compared to those achieved in other sizes along the reactor.

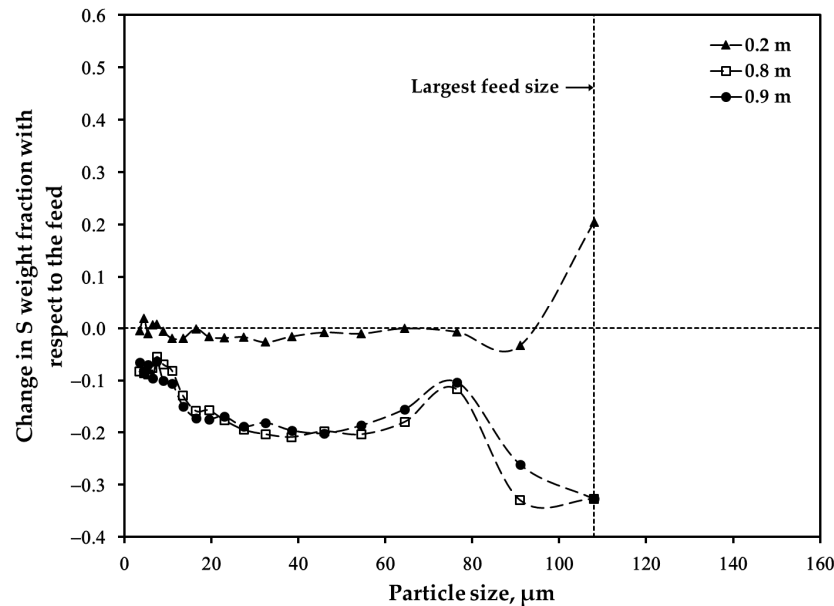


Figure 13. Changes in sulfur content in particles within the size fraction of 45–53 μm oxidized under 70 pct. O_2 in the process gas.

3.4. Distribution of Major Elements: Unsieved Concentrate after Oxidation

The study of the unsieved concentrate is relevant in the present context because it represents the typical feed to the industrial reactor. Furthermore, it is interesting to compare its behavior with those of the sieved fractions discussed above. Figures 14–16 show the distribution of copper, iron, and sulfur, respectively. Because particles in the unsieved concentrate were distributed over a wide range of sizes (0 to 154 μm), the experimental data in Figures 14–16 showed higher variability than that observed in the sieved fractions. Despite such difficulty, some trends were noted regarding the distribution of copper (Figure 14) and sulfur (Figure 16). The copper content (Figure 14) within all sizes increased along the reactor length. In addition, the higher the particle size was, the higher the increase in copper content. A relevant feature of Figures 14–16 is that no particles larger than the maximum size were detected in the feed (154 μm). Because the unsieved concentrate included particles from the <45 μm and 45–53 μm size fractions, the reaction paths discussed previously were expected to occur here as well. However, the wide range of sizes may have masked such phenomena.

Figure 15 shows that the iron content in the unsieved concentrate particles did not follow a clear trend. This is likely due to the wide range of sizes and compositions contained in the feed. Such results emphasize a general observation made in the discussion of the sieved fractions: the distribution of iron during oxidation was significantly more complex than those of copper and sulfur. This finding may represent a key feature to further investigate the reaction paths followed by particles during flash smelting, in particular, their possible association with particle fragmentation.

Finally, Figure 16 shows the changes in sulfur content in particles within the unsieved concentrate. The behavior of this response variable showed similar features to those observed in the sieved fractions (Figures 10 and 13): the amount of sulfur gradually decreased along the reactor. Also, the small sizes showed less reactivity than the intermediate and large sizes. Overall, the behavior of the unsieved concentrate was likely a combination of the reaction paths followed by the sieved fractions discussed previously. The experimental

data shown in Figures 14–16 point out the relevance of continuing the study of the reaction path under flash smelting conditions using sieved fractions of the original concentrate. This is because the behavior of unsieved concentrate particles provides information on the particle population as a whole. However, it may mask relevant phenomena occurring within specific sizes of the population.

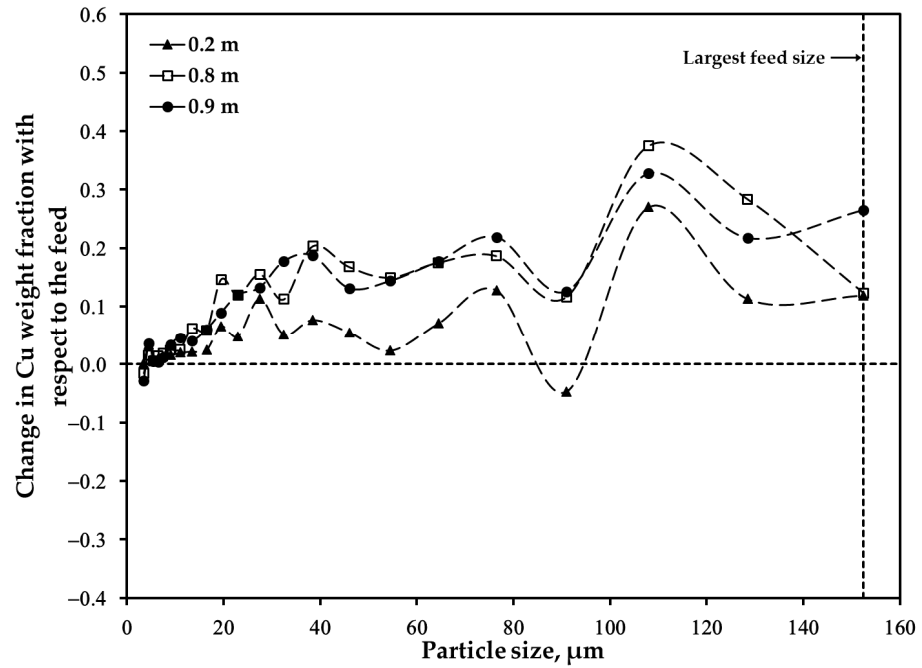


Figure 14. Changes in copper content in particles within the unsieved concentrate oxidized under 70 pct. O₂ in the process gas.

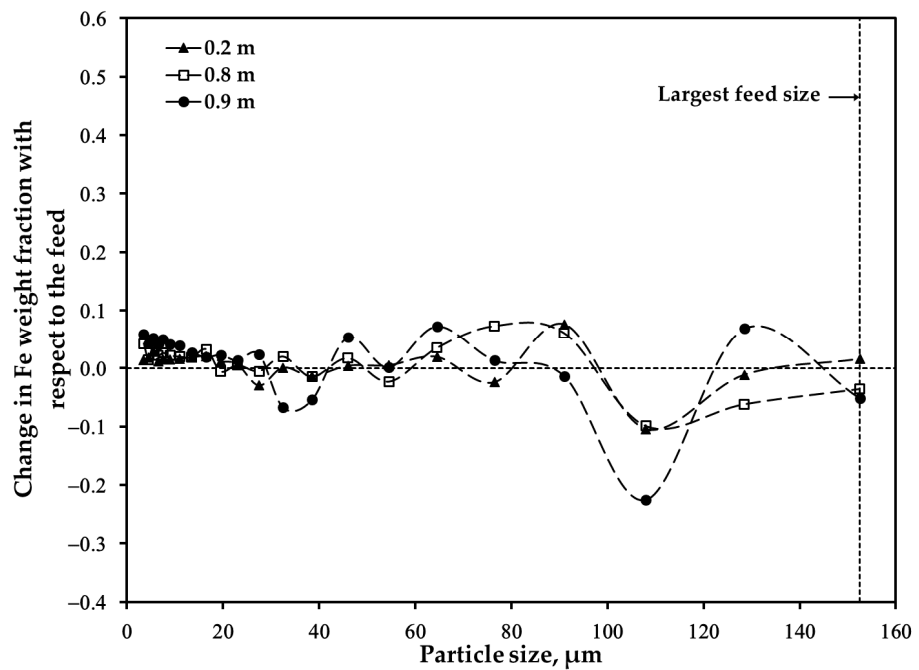


Figure 15. Changes in iron content in particles within the unsieved concentrate oxidized under 70 pct. O₂ in the process gas.

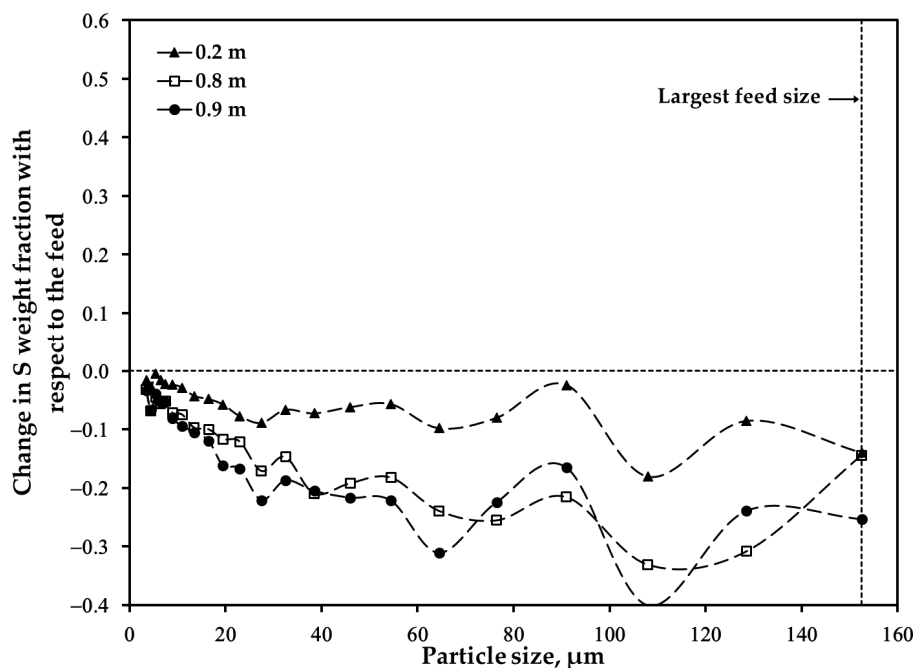


Figure 16. Changes in sulfur content in particles within the unsieved concentrate oxidized under 70 pct. O_2 in the process gas.

4. Concluding Remarks

The distribution of copper, iron, and sulfur during the oxidation of La Caridad copper concentrate particles under simulated flash smelting conditions was strongly dependent upon the size and chemical compositions of the initial particles. In contrast, the oxygen concentration in the process gas did not play a significant role in the range of 40%–70% in volume.

Because the initial content of the major elements in the particles was not uniform even within the sieved size fractions, the distribution of the major elements during oxidation showed various trends. Overall, the copper content increased and the sulfur content decreased within all sizes along the reactor length. This, in general, agreed with a reaction path of gradual oxidation of individual particles. However, the distribution of iron did not follow a general trend, as it increased, decreased, or remained unchanged depending on the particle size. This finding may represent a key feature to further investigate particle reaction paths during flash smelting, especially those related to particle fragmentation.

In general, the larger the particle size was, the greater the change in the content of the major elements within the population of particles was upon oxidation. The present work verified that particles within the size fraction of $<45 \mu\text{m}$ tended to follow a reaction path consisting of rapid melting followed by the collision and coalescence of reacting droplets during flight. In contrast, particles within the fraction of $45\text{--}53 \mu\text{m}$ tended to react individually. The experimental data with unsieved concentrate particles showed high variability and suggested a combination of both reaction paths. To help clarify the trends observed in this investigation, further research is necessary regarding the distribution of the chemical species within the particle population.

Author Contributions: Conceptualization, M.P.-T.; data curation, E.A.A.-H. and M.C.F.-S.; formal analysis, V.d.I.P.-O.; funding acquisition, M.P.-T. and V.R.P.-S.; investigation, V.d.I.P.-O. and V.R.P.-S.; methodology, M.P.-T. and V.R.P.-S.; software, V.d.I.P.-O., V.R.P.-S. and E.A.A.-H.; validation, V.R.P.-S.; visualization, E.A.A.-H. and E.A.V.-G.; writing—original draft, M.P.-T.; writing—review and editing, M.P.-T. All authors have read and agreed to the published version of the manuscript.

Funding: This research was funded by ANID FONDECYT INICIACIÓN 11201317.

Data Availability Statement: The data presented in this study are available on request from the corresponding author.

Acknowledgments: The authors are grateful to Komar Kawatra of Michigan Technological University for donating the electrical furnace used in the oxidation tests. Acknowledgments are also due to Antelmo Robles-Vega of Mexicana de Cobre, S.A., for providing the copper concentrate used in the present study.

Conflicts of Interest: The authors declare no conflicts of interest. The funders had no role in the design of the study; in the collection, analysis, or interpretation of data; in the writing of the manuscript; and/or in the decision to publish the results.

References

1. Sohn, H.Y.; Kang, S.; Chang, J. Sulfide Smelting Fundamentals, Technologies and Innovations. *Miner. Metall. Process.* **2005**, *22*, 65–76. [[CrossRef](#)]
2. Kim, Y.H.; Themelis, N.J. Effect of Phase Transformation and Particle Fragmentation on the Flash Reaction of Complex Metal Sulfides. In *The Reinhardt Schuhmann International Symposium on Innovative Technology and Reactor Design in Extractive Metallurgy*; Gaskell, D.R., Hager, J.P., Hoffman, J.E., Mackey, P.J., Eds.; TMS: Colorado Springs, CO, USA, 1986; pp. 349–369.
3. Jokilaakso, A.; Suominen, P.A.; Taskinen, P. Oxidation of Chalcopyrite in Simulated Suspension Smelting. *Trans. Inst. Min. Metall. Sect. C—Miner. Process. Extr. Metall.* **1991**, *100*, C79–C90.
4. Jorgensen, F.R.A.; Segnit, E.R. Copper Flash Smelting Simulation Experiments. *Proc Australas Inst Min Met.* **1977**, *261*, 39–46.
5. Jorgensen, F.R.A.; Koh, P.T.L. Combustion in Flash Smelting Furnaces. *JOM* **2001**, *53*, 16–20. [[CrossRef](#)]
6. Jorgensen, F.R.A. Cenosphere Formation During the Combustion of Pyrite. *Proc. Australas. Inst. Min. Metall.* **1980**, *276*, 41–47.
7. Jorgensen, F.R.A.; Zuiderwyk, M. Two-Colour Pyrometer Measurement of the Temperature of Individual Combusting Particles. *J. Phys. E* **1985**, *18*, 486–491. [[CrossRef](#)]
8. Jorgensen, F.R.A. Single-Particle Combustion of Chalcopyrite. *Proc. Australas. Inst. Min. Metall.* **1983**, *288*, 37–46.
9. Jokilaakso, A.; Ahokainen, T.; Teppo, O.; Yang, Y.; Lilius, K. Experimental and Computational-Fluid-Dynamics Simulation of the Outokumpu Flash Smelting Process. *Miner. Process. Extr. Metall. Rev.* **1995**, *15*, 217–234. [[CrossRef](#)]
10. Thomas, A.; Grace, J.R.; Samarasekera, I.V. Combustion of Copper Concentrate Particles in a Stagnant Gas Furnace. *Can. Metall. Q.* **2000**, *39*, 187–194. [[CrossRef](#)]
11. Kimura, T.; Ojima, Y.; Mori, Y.; Ishii, Y. Reaction Mechanism in a Flash Smelting Reaction Shaft. In *The Reinhardt Schuhmann International Symposium on Innovative Technology and Reactor Design in Extraction Metallurgy*; Gaskell, D.R., Hager, J.P., Hoffman, J.E., Mackey, P.J., Eds.; TMS: Colorado Springs, CO, USA, 1986; pp. 403–418.
12. Kemori, N.; Ojima, Y.; Kondo, Y. Variation of the Composition and Size of Copper Concentrate Particles in the Reaction Shaft. In Proceedings of the Flash Reaction Processes: Center for Pyrometallurgy Conference, Salt Lake City, UT, USA, 15–17 June 1988; pp. 47–68.
13. Kemori, N.; Denholm, W.T.; Kurokawa, H. Reaction Mechanism in a Copper Flash Smelting Furnace. *Metall. Mater. Trans. B* **1989**, *20*, 327–336. [[CrossRef](#)]
14. Pérez-Tello, M.; Parra-Sánchez, V.R.; Sánchez-Corrales, V.M.; Gómez-Álvarez, A.; Brown-Bojórquez, F.; Parra-Figueroa, R.A.; Balladares-Varela, E.R.; Araneda-Hernández, E.A. Evolution of Size and Chemical Composition of Copper Concentrate Particles Oxidized Under Simulated Flash Smelting Conditions. *Metall. Mater. Trans. B* **2018**, *49*, 627–643. [[CrossRef](#)]
15. Pérez-Tello, M.; Sohn, H.Y.; St. Marie, K.; Jokilaakso, A. Experimental Investigation and Three-Dimensional Computational Fluid-Dynamics Modeling of the Flash-Converting Furnace Shaft: Part I. Experimental Observation of Copper Converting Reactions in Terms of Converting Rate, Converting Quality, Changes in Parti. *Metall. Mater. Trans. B* **2001**, *32*, 847–868. [[CrossRef](#)]
16. Themelis, N.J.; Wu, L.; Jiao, Q. Some Aspects of Mathematical Modeling of Flash Smelting Phenomena. In Proceedings of the Flash Reaction Processes: Center for Pyrometallurgy Conference, Salt Lake City, UT, USA, 15–17 June 1988.
17. Schlesinger, M.E.; Sole, K.C.; Davenport, W.G.; Alvear Flores, G.R.F. Chapter 6—Flash smelting (Davenport et al., 2001). In *Extractive Metallurgy of Copper*, 6th ed.; Schlesinger, M.E., Sole, K.C., Davenport, W.G., Alvear Flores, G.R.F., Eds.; Elsevier: Amsterdam, The Netherlands, 2022; pp. 119–141, ISBN 978-0-12-821875-4.
18. Chaubal, P.C.; Sohn, H.Y. Intrinsic kinetics of the oxidation of chalcopyrite particles under isothermal and nonisothermal conditions. *Metall. Trans. B* **1986**, *17*, 51–60. [[CrossRef](#)]
19. Pérez-Fontes, S.E.; Pérez-Tello, M.; Prieto-López, L.O.; Brown, F.; Castellón-Barraza, F. Thermoanalytical study on the oxidation of sulfide minerals at high temperatures. *Miner. Metall. Process.* **2007**, *24*, 275–283. [[CrossRef](#)]

Disclaimer/Publisher’s Note: The statements, opinions and data contained in all publications are solely those of the individual author(s) and contributor(s) and not of MDPI and/or the editor(s). MDPI and/or the editor(s) disclaim responsibility for any injury to people or property resulting from any ideas, methods, instructions or products referred to in the content.